Curved mineral platelets in bone

H P Schwarcz, Nadine Nassif, Viktoria Kovacs Kis

Acta Biomaterialia xxx (xxxx) xxx

Contents lists available at ScienceDirect

Acta Biomaterialia

journal homepage: www.elsevier.com/locate/actbio

Full length article

Curved mineral platelets in bone

H.P. Schwarcz[a,b,*], Nadine Nassif[c], Viktoria Kovacs Kis[d,e]

[a] School of Earth, Environment and Society, McMaster University, Hamilton, Ontario, Canada
[b] School of Biomedical Engineering, McMaster University, Hamilton, Ontario, Canada
[c] CNRS, Sorbonne Université, Collège de France, Laboratoire Chimie de la Matière Condensée de Paris (LCMCP), F-75005 Paris, France
[d] HUN-REN Centre for Energy Research, Konkoly-Thege Miklós u. 29-33, H-1121 Budapest, Hungary
[e] Department of Mineralogy, Eötvös Loránd University, Pázmány Péter sétány 1/c, H-1119 Budapest, Hungary

ARTICLE INFO

Article history:
Received 12 March 2024
Revised 24 May 2024
Accepted 30 May 2024
Available online xxx

Keywords:
Apatite
Transmission electron microscopy
Ion beam milling
Folding
Developable surface
Stacks

ABSTRACT

Bone is a composite material principally made up of a mineral phase (apatite) and collagen fibrils. The mineral component of bone occurs in the form of polycrystalline platelets 2–6 nm in thickness. These platelets are packed and probably glued together in stacks of two or more, ranging up to >30 platelets. Here we show that most of these stacks are curved flat sheets whose cylindrical axes are oriented parallel to the long axes of collagen fibrils. Consequently, the curvature of the platelets is not detectable in TEM sections cut parallel to the collagen fibril axes. The radius of curvature around these axes ranges from about 25 nm (the average radius of the collagen fibrils) to 100′s of nm. The shapes of these curved forms contribute to the compressive strength of bone.

Statement of significance

Bone, the material of which bones are made, is mainly composed of a protein, collagen, and the mineral apatite (calcium phosphate). The crystals have long been known to be flat plates about 5 nanometers (nm) thick. Here we show that the crystals are bound together in curved platelets with a radius of curvature between 25 and several hundred nm, which weave between fibrils of collagen. Some platelets wrap tightly around fibrils. The platelets form stacks of from two to up to 30. The crystals in the platelets are all oriented parallel to the cylindrical fibrils even though most crystals are not in contact with collagen. These curved structures provide greater strength to bone.

1. Introduction

Bone is a composite material largely composed of equal volumes of mineral (apatite) and collagen fibrils. Since the late 20th century studies of the ultrastructure of bone were carried out by transmission electron microscopy (TEM) to examine sections of bone prepared by ultramicrotomy [1–4]. Based on TEM study of microtome-cut sections, it was widely believed that the mineral is largely or wholly enclosed inside collagen fibrils [5–7], an idea which was reinforced by the study of mineralized turkey leg tendons in which this is actually true [8,9].

Ion milling was first employed to examine bone in the 1980′s [10] but this method did not become more widely used until the 2010′s [11–14]. Using this method, it was possible to show that the mineral phase of bone mainly lies outside the fibrils in the form of mineral platelets (MPs) 2 to 6 nanometers (nm) in thickness which surround the fibrils and lie in the spaces between them [13]. This clearly seen in sections cut normal to the axes of collagen fibrils (CFs) (Fig. 1a).

The fibrils themselves appear as approximately circular hole-like features in the sections. Using electron energy loss spectroscopy (EELS), Lee et al. [16] showed that C and N were present in holes in sections cut with a microtome, showing the presence of collagen. In ion milled sections much of the collagen in these holes is removed by the Ar^+ions used to cut the section.

TEM images of ion-beam milled sections of bone cut parallel to the CF axes (Fig. 1b) show the presence of weakly electron-absorbent bands 40 nm wide which define gaps in the structure of the collagen fibrils. They contain significantly high concentrations of Ca and P [11,17]. Many publications over the last decades state that the mineral component of bone largely occurs in these gap zones, e.g., [18–22], while some recent papers suggest that both

* Corresponding author.
E-mail address: schwarcz@mcmaster.ca (H.P. Schwarcz).

https://doi.org/10.1016/j.actbio.2024.05.047
1742-7061/

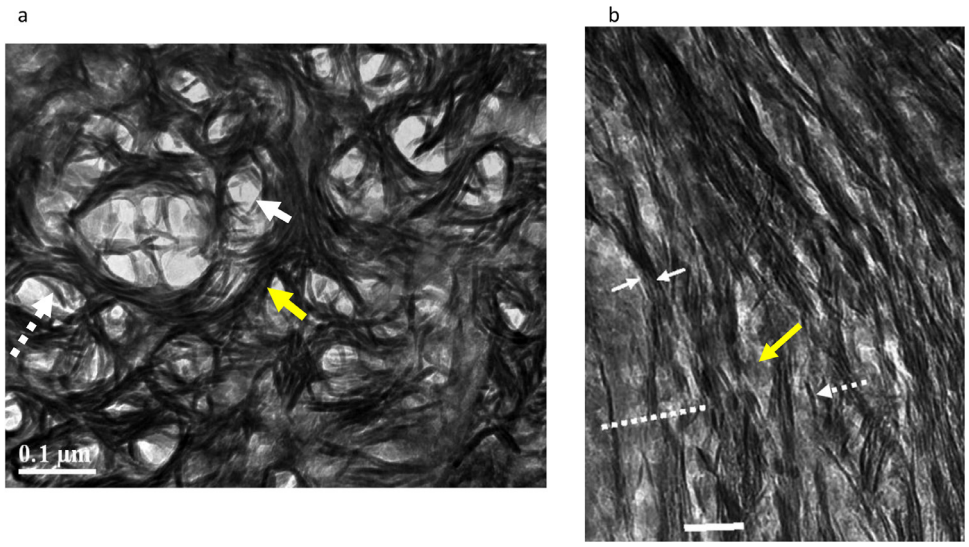

Fig. 1. TEM images of ion milled sections of human cortical bone: a) section cut normal to axes of collagen fibrils; solid arrow: collagen fibril cross section; dashed arrow: single mineral platelet; yellow arrow: stack of mineral platelets; scale = 100 nm; b) section cut parallel to collagen fibril axes: dashed arrow: mineral platelet; two solid arrows: stack of mineral platelets; dashed line highlights an electron dense band in the collagen gap zones of multiple superimposed fibrils; yellow arrow: space between two stacks of MPs; scale = 50 nm; from [15]. (For interpretation of the references to color in this figure legend, the reader is referred to the web version of this article.)

intrafibrillar and extrafibrillar mineral are present in bone (e.g., [23,24]). Micheletti et al. [17] confirm, using tomography, that intrafibrillar mineral exists at these sites although some gap zones had none; however they fail to find crystals of apatite at these sites. Dark field analyses [25] also showed that no significant amount of apatite crystals resides in these gaps. The precise nature of the Ca,P-rich material occurring in gap zones of CFs is not definitively known as yet.

Mineral occurs as platelets surrounding and filling the space between CFs. The spaces visible between stacks of MPs in sections cut parallel to the CFs (e.g., yellow arrow in Fig. 1b) are also filled with apatite in the form of approximately flat-lying MPs which completely surround the CF. They are not recognizable as platelets in this orientation, however.

Note that Fig. 1a and b are not exceptional views of features of ion-beam milled sections of bone. They have been seen in many sections of cortical and trabecular bone, in bones of humans, cows, pigs and many other vertebrates (Schwarcz, in preparation).

2. Methods

All TEM images in this paper were obtained on sections which had been prepared using ion beam milling. Methods for this procedure have been summarized in [13] and [26]. Fig. 1a was obtained using a Zeiss NVision40 gallium focused ion beam (FIB) milling machine instrument and the image was obtained on a JEOL 2010F scanning transmission electron microscope, operated at 200 keV. The sample shown in Figs. 1b, 2a,b, 3 and 4 were prepared on a Fischione 1010 low angle ion milling and polishing system equipped with a cryostage. The images were obtained on a Philips CM12 electron microscope operated at 120 keV and on a FEI Titan 80–300 Cryo operated in the range from 80 to 300 keV. Fig. 2c,d were of a sample prepared on the above FIB device, and imaged on a Titan 80–300 microscope operated at 300 keV, using high-angle annular dark-field (HAADF) electron optics. All these instruments are at McMaster University in the Canadian Center for Electron Microscopy (CCEM). Fig. 5a,b were obtained on a FEI Themis G2 Cs corrected microscope (FEI, Thermo Fischer, Schottky FEG electron source).

For Fig. 7a, a sample of bone was ground in a ceramic mortar, then treated with commercial, undiluted bleach (NaClO solution) for 24 h at room temperature, rinsed with water, suspended in 100 % EtOH, spun for 10 min on a centrifuge; supernate was transferred to a carbon-coated Cu TEM grid; see [27]; sample for Fig. 7b was similarly prepared, but treated only with chloroform ($CHCl_3$). TEM images were obtained on the Philips CM12 microscope.

2.1. Samples

Samples of bone from which TEM sections were obtained are as follows: Figs. 1, 2a,b and 3: FIB section prepared from samples extracted during preparation for insertion of screws into femora of patients at the Hospital for Special Surgery and New York-Presbyterian Hospital, as described in [28]; Fig. 1b: Section of femoral diaphysis of a healthy 60 y old human male remaining from an allograft procedure, provided by Dr. N Colterjohn, McMaster University; see [13]; Fig. 2c,d, Fig. 10: cortical bone from the femur of a healthy, 19-year-old male obtained with ethical approval as a by-product of restorative surgery; see [26]; Fig. 4: section of femoral diaphysis from bovid (from local source). Fig. 5: Cortical bone from human femur, courtesy of Prof. Szekanecz, University of Debrecen. Material for samples in 7a: same as Fig. 10; 7b: same as Fig. 5.

3. Results

The experimental results on which this paper is based are largely published TEM images of bone as well as some unpublished data from as-yet unpublished studies in our laboratory.

Schwarcz et al. [29] used dark-field (DF) illumination to show that discrete crystals about 30 nm in length were illuminated inside MPs, showing that the MPs were polycrystalline. Independently, Scherrer-method analyses of the X-ray diffraction patterns of bone showed that the average length of single crystals along their c-axes ((002) reflection) was about 34 nm [30], consistent with the dark-field image data.

Most of the MPs are arranged in stacks of multiple platelets (between 2 and 30) in which the minimum space between any two adjacent MPs is < 1 nm. As a result, the space between the CFs is filled with curved stacks of multiple MPs. As well, discrete, densely-packed “rosettes” of stacked MPs form elliptical masses

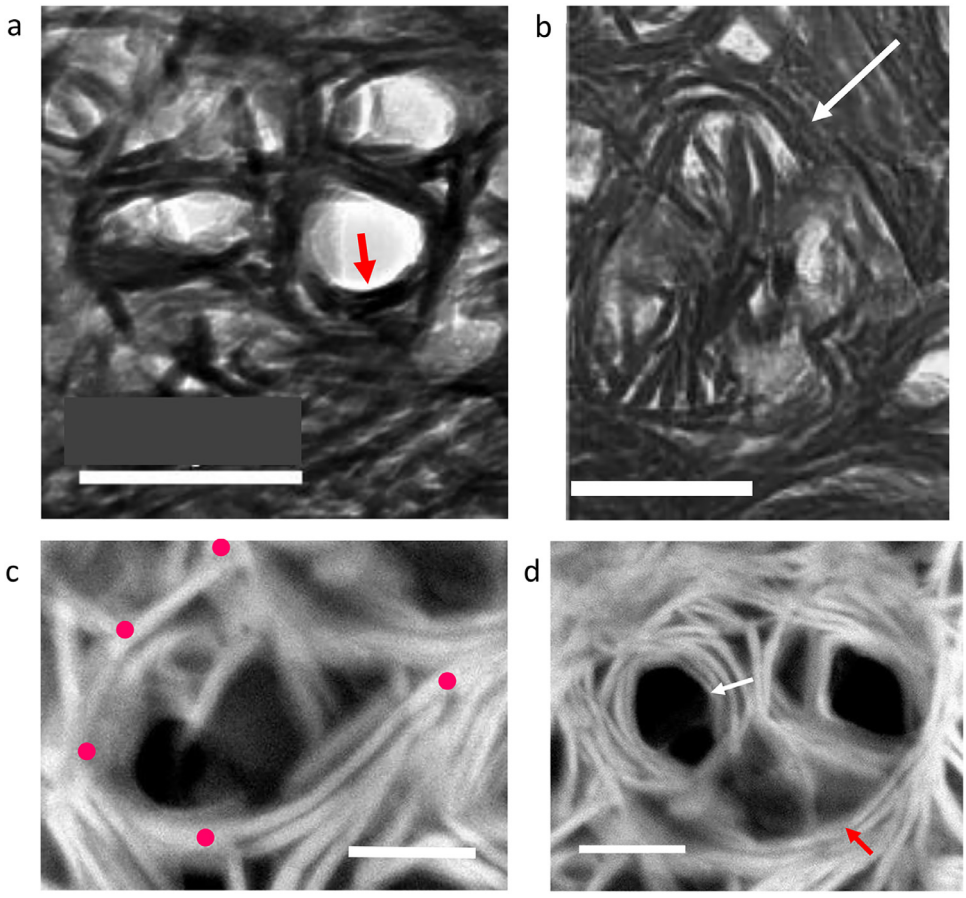

Fig. 2. TEM images of ion beam milled sections of cortical human bone: a) bright field image of three collagen fibrils, surrounded by close-fitting curved mineral platelets (red arrow); b) triangular arc of mineral platelets (arrow) ~ 180 nm across; c: HAADF image; red dots outline open arc of mineral platelets; d) HAADF image; approximately circular arc (red arrow) surrounding two collagen fibrils; left-hand fibril shows three ranks of mineral platelets surrounding fibril (white arrow) From [26]. Scales: 100 nm. (For interpretation of the references to color in this figure legend, the reader is referred to the web version of this article.)

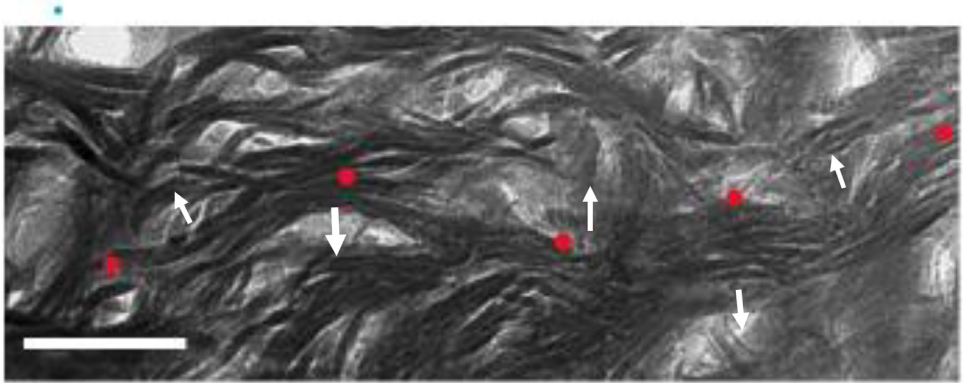

Fig. 3. TEM of human cortical bone sectioned normal to the axes of collagen fibrils, showing a complex of arcs (outlined by red dots) made up of several mineral platelets whose sense of curvature changes along the feature; arrows point towards hypothetical centers of fitted circular cylinders. Scale = 100 nm. (For interpretation of the references to color in this figure legend, the reader is referred to the web version of this article.)

scattered through bone; these are only clearly recognizable in sections cut normal to the CFs [31] and have been related to features identified by McKee et al. [32] as mineral tessellation.

3.1. Characteristics of the mineral platelets

The mineral component of bone which surrounds and lies between the CFs is entirely in the form of stacks of thin platelets. In this paper we shall investigate the form of these platelets and the stacks in which they occur. Electron tomographic studies have been able to obtain only sketchy images of the 3D form of MPs [33–36] and have so far failed to provide definitive notions of their form. Other instrumental analyses reveal some characteristics of the MPs. Selected-area electron diffraction (SAED) studies show that the c-axes of the apatite crystals are oriented approximately parallel to the axes of the CFs [13,37]. Also, small-angle X-ray scattering (SAXS) shows that the average thickness of the MPs remains constant in mm-sized regions of cortical bone [38]. Here we shall mainly use TEM images of ion-beam milled sections. Some will be bright field images like Fig's 1a,b in which mineral platelets are

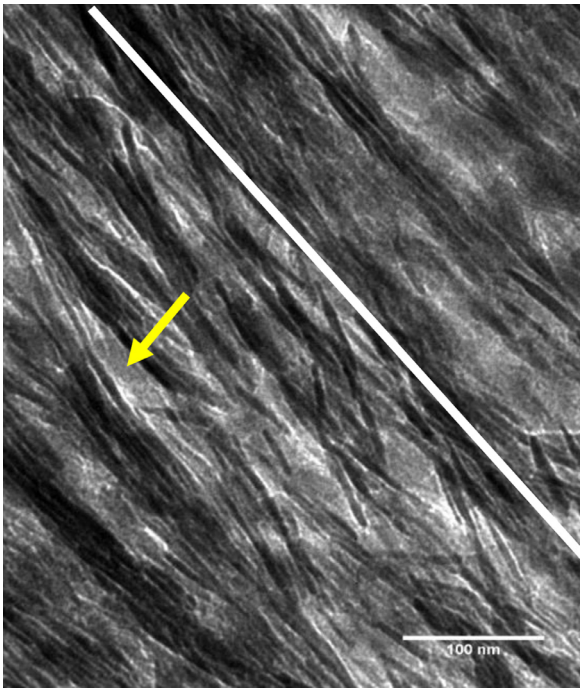

Fig. 4. TEM image of section of bovine cortical bone, cut parallel to long axes of collagen fibrils; white line defines this axis. Yellow arrow: gap between two stacks. Scale = 100 nm. (For interpretation of the references to color in this figure legend, the reader is referred to the web version of this article.)

dark against a light background; others will be high-angle annular dark field (HAADF) images in which the mineral appears light against a dark background.

Images such as Fig. 1a and b show that the appearance of MPs varies greatly depending on the orientation of the section with respect to the CF axes. Here we shall try to derive the three-dimensional physical form of MPs in cortical bone from 2D images of sections cut parallel and perpendicular to their CF axes.

3.2. Mineral platelets viewed normal to collagen fibril axes

In sections cut normal to the CF axes such as Fig. 1a, essentially every MP appears to be curved. In stacks of MPs, all are curved in parallel. The curvature is approximately circular, with the smallest radii of curvature (R_c) found in MPs wrapping around CFs (Fig. 2a,d).

In TEM sections of bone, the CFs have average diameters of 50 nm [39] although unmineralized collagen fibrils can have larger diameters [40]. The radii of curvature of the MPs adjacent to them are $\geq$ 25 nm. In the stacks of MPs surrounding the CFs the R_c values gradually increase away from the CF. The circular form of these curved MPs is determined by the cylindrical shape of the CF which they surround. It is likely that the MPs immediately adjacent to CFs were deposited at these loci because the collagen fibril surface acted as an epitaxial locus for growth of apatite [41–43]. In [17] are shown images of ion-beam milled three-dimensional needle-shaped sections of osteonal bone in which curved MPs surrounding CFs can be clear resolved (e.g., their Fig. 2F).

Larger circular or curved arcs of MP stacks occur between the CFs (Fig. 2b), with R_c's ranging up to 100′s of nm. These larger arcs continue to be approximately circular, although their circular form is clearly not determined by proximity to a cylindrical target surface acting as an epitaxial site.

Many curved shapes are more complex than a simple circular arc. Fig. 2c shows an open curved arc surrounding a CF. The arc is composed of three platelets: the lower one is ~180 nm long, while the upper two platelets are 40 and 50 nm long. Some of these MPs may, however, be connected at a lower or higher level in the bone which was sectioned. Additional MPs form a stack with the lowermost of these three platelets. In Fig. 2d shows a quasi-circular arc (red arrow) composed of three platelets 215, 130 and 50 nm long. Additional, parallel MPs are stacked with all of these. A CF occurring within the quasi-circular structure of Fig. 2d (white arrow) is

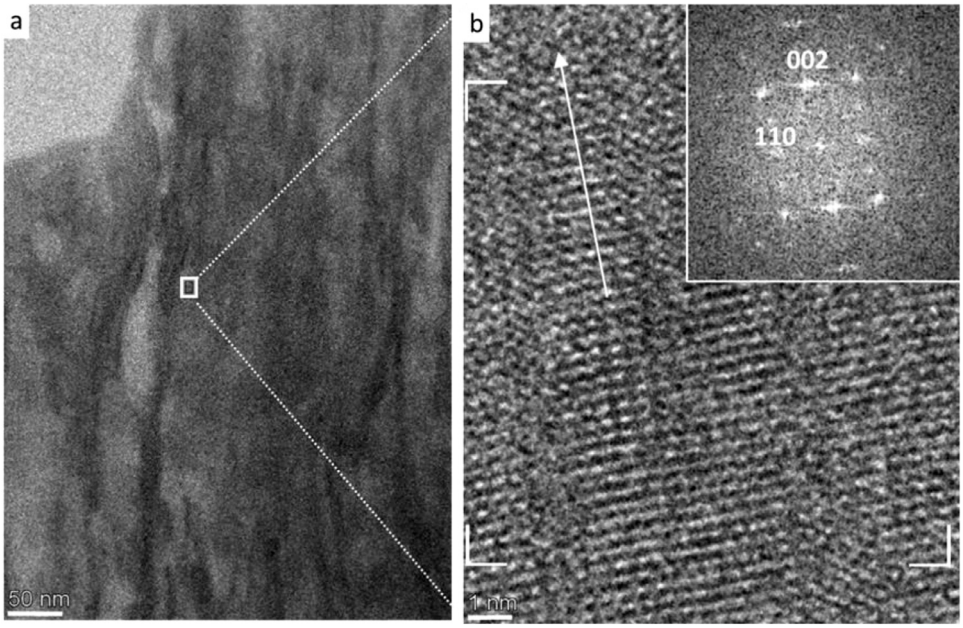

Fig. 5. Demonstration of presence of mineral between stacks: a. Bright field TEM image of ion-milled section of human femur; scale = 50 nm; b) HRTEM image of the area indicated in a, scale = 1 nm. Fourier transform of the area indicated with white corners is in the insert. According to the Fourier transform, apatite is viewed down the normal of the flat plane (010). White arrow is parallel to apatite c axis, which roughly coincides with the long axis of CFs. (For interpretation of the references to color in this figure legend, the reader is referred to the web version of this article.)

enwrapped by correspondingly smaller circular MPs. Generally, the longest arcs are defined by stacks of two or three close-spaced MPs

Some MPs change their sense of curvature and have inflection points (Fig. 3); generally, the R_c's of these platelets are very large. In Fig. 3 arrows point in the direction of curvature of the successive arcs which make up a complex of several MPs stacked together.

Some MPs (<5 %) are almost planar but even these have slight wiggles in them. It appears that, when viewed in sections cut normal to the CFs, all MPs are curved to varying extents.

3.3. Mineral platelets viewed parallel to collagen fibril axes

In Fig. 1b we see that MPs are also collected into stacks, but the degree of curvature is much less. In Fig. 1b all the stacks conform approximately to one curve with $R_c \sim 730$ nm. Fig. 4 shows another image in which there is no curvature of the MPs, although some of the MPs are misaligned with respect to the principal direction in the section. This degree of straightness is seen in all sections cut parallel to the CFs [13,15,26] and varied vertebrate species (unpublished results).

The average open space between the most prominent stacks of MPs is 34 ± 20 nm wide. This is because they are surrounding mineral-free CFs with radii of ~50 nm. However, curved MPs must also extend over these apparently open regions since MPs completely surround the CFs. They are unresolvable along these open spaces, because MPs can only be recognized, at low magnification, as electron-dense linear features (dark in a bright field image) when they are viewed edgewise. The effect is the same as viewing a flat pane of glass normal to the pane vs edgewise. However, the presence of these flat-lying MPs between the stacks can be seen using high resolution TEM (HRTEM) on a region between two stacks (Fig. 5)

Darker patches 40 nm wide within these open spaces between stacks define sites where Ca and P are present in the gap zones of the CFs. Schwarcz et al. [29] suggested these could be regions of amorphous calcium phosphate (ACP). Conversely, ^{31}P solid-state NMR studies indicate that ACP only exists around the mineral crystalline core [44], although apatite is not present in gap zones in studied bone samples.

3.4. Collective 3D view of bone ultrastructure

By combining images such as Fig. 1a and b, we now see that the 3D structure of normal bone would at least partly consist of cylindrical curved sheets whose axes of curvature are consistently parallel to the axes of the collagen fibrils. The technical (mathematical) name for these sheets is “developable surfaces", defined to be two-dimensional surfaces which have zero curvature in one direction and are curved in the direction normal to that. This is schematically illustrated in Fig. 6.

We have only sketched a few of the MPs that would be in this field of view and have only sketched the extent to which these would be stacks of multiple platelets. The thin blue lines define the position and orientation of a section cut parallel to the collagen fibril axes. In such a section the MPs would appear as straight linear features as in Fig. 4. In a section normal to that plane and to the CF axes, the MPs would appear as curved linear features and the CFs would appear circular in cross section.

4. Discussion

We see that the extrafibrillar volume of bone is filled with curved, polycrystalline platelets of mineral stacked together at distances as close as < 1 nm. The crystals inside these platelets are oriented so that their c-axes are approximately parallel to the adjacent collagen fibrils. These are the forms that the mineral of bone is precipitated in as it grows from the extracellular fluid. This raises some questions:

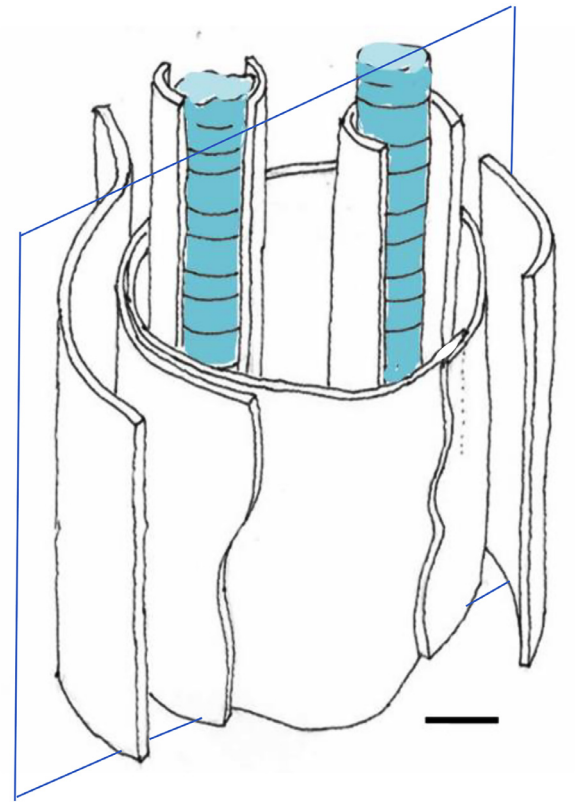

Fig. 6. Schematic drawing of a section of bone. Curved white sheets are mineral platelets (with edges shown as straight lines). Blue cylinders are two collagen fibrils. Blue line shows plane of a section parallel to the axes of the collagen fibrils. Scale = 50 nm. (For interpretation of the references to color in this figure legend, the reader is referred to the web version of this article.)

4.1. Why are the MPs curved?

Curvature is clearly advantageous from the standpoint of ensuring the largest volume of mineral to exist between the CFs. This increases the physical strength of the CF-MP assemblage. It is relevant, however, to compare these images with images obtained by grinding samples of bone to a fine powder, deproteinizing the powder with an oxidant such as bleach (NaClO), and dispersing the residual mineral particles on a carbon-coated TEM grid [45] (Fig. 7).

Fragments of MPs (larger than the size of single crystals) lie flat on the carbon-coated grid; a few standing edgewise are quite straight, unlike the images seen in Figs. 1a, 2. No curved flakes at all are seen in other published images of deproteinized bone powder [27,46,47].

The fact that the MPs lie flat when surrounding protein has been oxidized away implies that they do not have a spontaneous tendency to be curved. Rather, it seems more likely that these thin flakes and even stacks of them are passively curved to accommodate the space available for them. Even when multiple plates are bound together in stacks, they maintain this degree of flexibility. A fraction of the MPs (about 1/3 or less) are closely wrapped around collagen fibrils where they may have crystallized epitaxially; when the collagen is oxidized away, apparently these also unroll into flat plates.

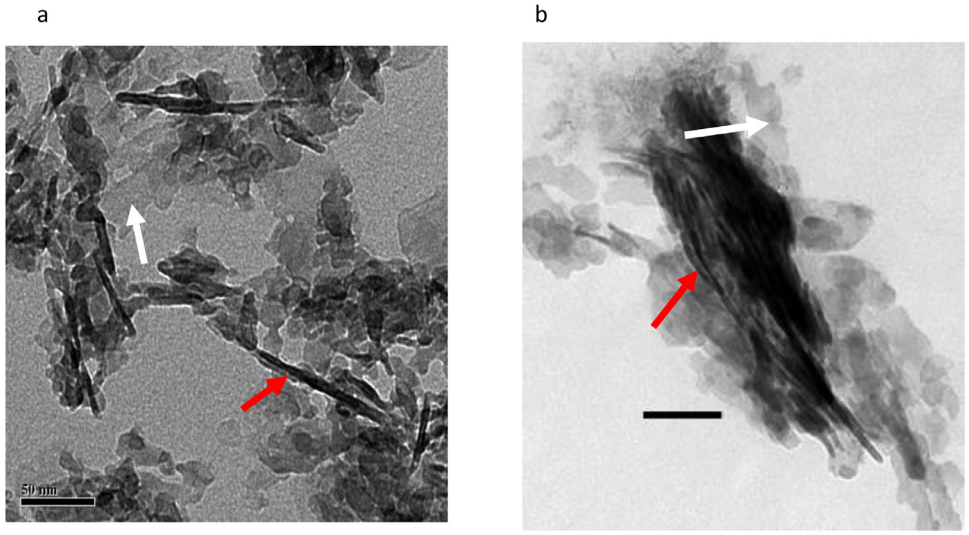

Fig. 7. TEM images of powdered bone, Fragments of MPs (white arrow) lie flat on underlying carbon grid. Some fragments standing edgewise (red arrow) are also flat. a) human cortical bone deproteinated with bleach (NaClO) (from [15]); b) sheep bone, treated with chloroform ($CHCl_3$). Scale = 50 nm in both images. (For interpretation of the references to color in this figure legend, the reader is referred to the web version of this article.)

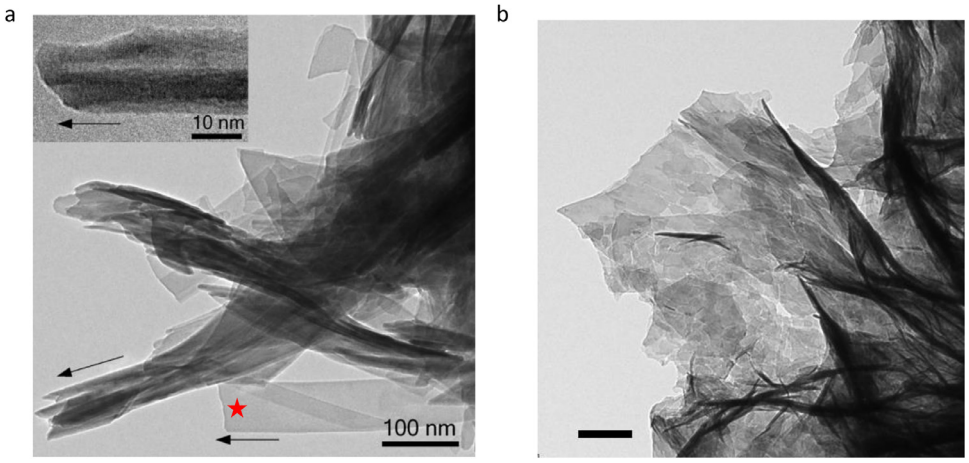

Fig. 8. Sheets (platelets) of synthetic CO_3 apatite produced by vapor-diffusion of NH_3 into low-pH aqueous solution of Ca^{2+}, PO_4^{3-} and HCO_3^{2-} ions : a. Sheets are folded along c axis (arrow). From [48], Fig. 4; red star: flat sheet; scale = 100 nm; inset: higher magnified view of a folded platelet with visible 002 lattice planes; b : TEM image showing flexibility of polycrystalline sheets of apatite; scale = 200 nm. (For interpretation of the references to color in this figure legend, the reader is referred to the web version of this article.)

For the MPs surrounding CFs, at least, their curved form is determined by the shape of the fibril around which they have grown, but this would not account for the curvature of most of the MPs which lie between the CFs. The proximity of fibrils and MPs causes them to take curved configurations. Nassif et al. devised a method for growing apatite crystals with compositions somewhat similar to that of bone [48]. In Fig. 4 of their paper, mineral platelets (i.e., much larger than individual crystals as determined by Scherrer analysis) are folded along axes parallel to the (001) axis (Fig. 8a); these curved forms resemble cylindroidal curved platelets in bone (Fig. 5). Most of the platelets in Fig. 8a are curved because at their other ends (not seen in this figure) they are crowded together in a bundle of similar plates. A flat platelet is shown at the bottom of the image (red star).

The consistent orientation of the c axes parallel to the axes of curvature suggests that this is the weakest zone in these plates and therefore the preferred axis of folding. This fact has an interesting consequence as we shall see below. The slight degree of curvature in varying directions seen in some MPs (Fig. 3) is explicable by the fact that the MPs are very flexible (Fig. 8b). They take whatever form the space available to them allows, resulting in additional folds, but still with cylindroidal axes parallel to (001).

4.2. Why are the axes of curvature parallel to the collagen long axes?

All the curved sheets appear to be curved along axes parallel to or close to the axes of the collagen fibrils. This is because, as they grow, they also encircle CFs. This requires the axes of curvature to be parallel to the CFs. If the spaces between CFs had been larger, it would have been possible for the MPs to curve around cylindrical axes pointing in any direction, but the limited space available in bone does not allow this.

An important characteristic of bone is seen in selected area electron diffraction (SAED) images of TEM sections of bone (Fig. 9). Reflections from the c-axes ((002) and (004)) form two opposed clusters with dispersions of about $\pm$ 15^0 around the axis of the CFs.

This alignment which has been noticed by many researchers [37,49,50] has generally been attributed to the fact that the apatite crystals were nucleated on collagen fibrils. We have shown that

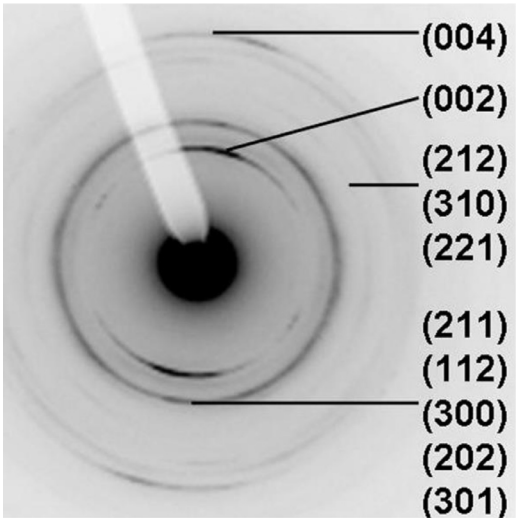

Fig. 9. Selected-area electron diffraction pattern from a sample of human femoral bone; the long axis of the bone was oriented parallel to the vertical edge of the image. The (002) and (004) reflections are clustered around a line almost parallel to the bone axis. From [13] Fig. 1b.

this is not always true, and most of the platelets are not found next to collagen but rather growing in the spaces between CFs. There is no suggestion that they are formed at such sites and migrate away to fill the space between CFs. Also, most CFs have MPs attached to their surface (Fig. 2b,d), so the collagen itself could have no influence on the crystallization of MPs further away.

One can only tentatively speculate on the reasons for this alignment. One possibility is that either the apatite crystals themselves or organic molecules attached to them might have an electrical dipole moment which could interact with an electrical field associated with the collagen molecules. This could cause the crystals to rotate into alignment with the fibrils. However, most of the MPs are > 20 nm away from the CFs and, if a dipole moment existed on the CF, it is doubtful that its electrical field would be able to move the MPs located at such distances.

A simpler explanation might arise from the curvature of the MPs. We saw in Fig. 8a that the mineral plates bend in a cylindroidal manner with the c axis of the crystals parallel to their axis of curvature. But we also see (e.g., in Fig. 2a,d) that the MPs curve around the CFs. As they curve, the axis of curvature must also be parallel to the crystallographic c-axis of the MPs. The result is that the c-axes of the apatite crystals are aligned parallel to the CFs. As well, some MPs will be aligned this way because they grew epitaxially on the CFs. Thus, crystal alignment in bone may be for two discrete reasons.

4.3. How do stacks of MPs form?

Mineral platelets, both those around collagen fibrils, and those between fibrils, occur closely associated in stacks; these have been recognized by many other people studying bone both in TEM [33,51], in FIB-SEM [52], in small angle X-ray scattering [53,54] and in atomic-force microscopy [55].

Wang et al. [44] showed that suspensions of synthetic carbonated- or bone apatite self-assembled into stacks of up to 30 platelets in the absence of collagen or any other binding agents. By using nuclear magnetic resonance analysis, they showed that both apatite crystals present a layer of ACP on their surfaces. Using wide angle X-ray diffraction (WAXD) measurements of the relative intensities of (002) compared to the merged $2\theta = 31.9^0$ peak (CuKα radiation) they conclude that the presence of an amorphous layer increases the tendency of the MPs to form coherent stacks with mutually aligned c-axes in water.

Pang et al. [27] showed that the existence of stacks in bone contributed significantly to the compressive strength of bone. Under compression testing, bone treated to remove collagen but leaving other organic molecules intact was initially as strong as untreated bone. They inferred that there must be an organic glue holding the plates together. This glue molecule could also nucleate the growth of an additional platelet on the surface of an existing one, with the same lattice orientation. This would help account for the parallel orientation of c-axes of crystals in stacks (which is also indicated by the clustering of c-axes orientations in SAED patterns).

Other studies have suggested the presence of organic glue contributing to the strength of bone (e.g., [56]). Pang et al. [27] show, however, that the diameters of all proteins are too large (>2.3 nm) to fit in the < 1 nm wide gap between adjacent plates in stacks of MPs.

Stacks of two or more platelets form curved surfaces with widely variable radii of curvature. The smallest are stacks around CFs where the inner platelet has a radius of curvature determined by the diameter of the CF, and the next outer plate has a correspondingly larger R_c (Fig. 2d).

4.4. Relation to larger scale features; hierarchical structure

Many studies of the nanoscale structure of bone have been done using FIB-SEM or SEM studies of exposed surfaces of bone

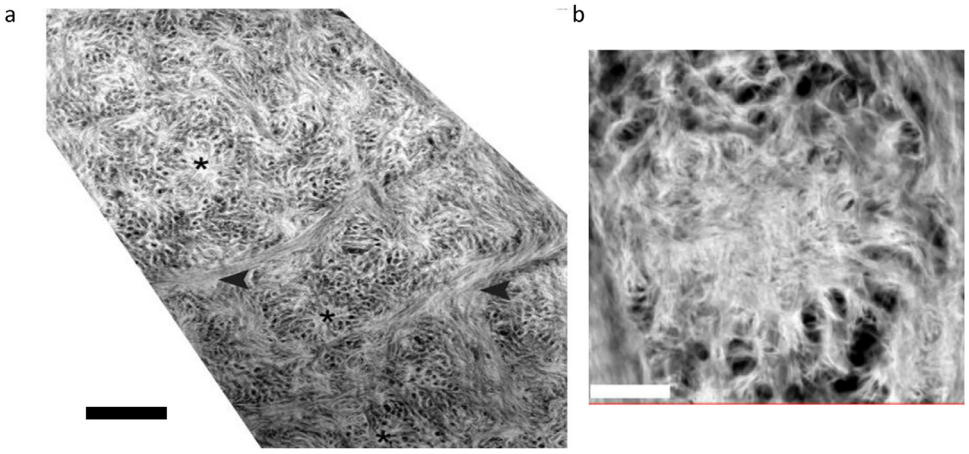

Fig. 10. a) HAADF TEM image of ion-beam milled (FIB) section of femoral human cortical bone, cut normal to axes of collagen fibrils. Stars indicate two rosettes. Magnification is much lower than in Figs. 1, 2, 3. Scale = 1 µm; from [26]; b) single rosette; from [36], Fig. 7a(4); scale = 200 nm.

[32,52,57]. Binkley et al. [31] identified dense ellipsoidal patches which resembled "rosettes" of densely clustered MPs that had been previously identified by Grandfield et al. [26] in TEM images of ion-beam milled sections made at lower magnifications than Figs. 1, 2, 3 (Fig. 10).

Rosettes appear to comprise a few percent of the total volume of bone. They are barely perceptible in sections cut parallel to the axes of CFs although Binkley et al. [31] were able to identify them as "elongate ellipsoids" in FIB-SEM images of bone. We have not discussed the structure of these rosettes here because we do not yet possess sufficiently detailed images of them to discern the relationships between MPs inside them. They appear to be deficient in collagen compared with the remaining volume of bone. The fact that they are irresolvable in CF-axis-parallel sections suggests that the MPs in the rosettes are not distinctively formed compared to those in the surrounding material. Consistently using in vitro models, the precipitation of such crystals shape (spherulites) was proposed to occur when homogenous nucleation (versus heterogenous on collagen) occurs possibly in spaces lacking confinement [43,58].

McKee et al.[32]. and Buss et al. [57] identified "tessellations" of bone, ellipsoidal volumes which are isolated from one another by faintly defined boundaries that appear dark in FIB-SEM images and therefore must be zones of lower mineral concentration; this is discussed in detail by [36].

Tessellations are not recognizable in higher-magnification TEM images such as we have been referring to in this paper. This is consistent with a notion that bone is constructed hierarchically [59], and that the ellipsoidal features can exist on a larger scale in a medium which is composed of curved mineral platelets. Nevertheless, the high-magnification ("higher hierarchical level") features which we have described in this paper may contribute significantly to the gross physical behavior of bone, such as compressive strength and toughness [15,27,60,61].

5. Conclusions

The earliest studies of bone by TEM using sections prepared with ion-beam milling [12,13] showed that apatite occurred in well defined, curved platelets partly wrapping around collagen fibrils. However, the curvature of these platelets was hardly commented on by these authors, and especially not the curvature of the platelets which lay between fibrils. In this paper we have presented novel insights into the curvature of the MPs, focusing specifically on the question of why the MPS are consistently curved and how they achieved this status. We have especially emphasized the fact that the axes of curvature are always parallel to the collagen fibril axes, and that the radii of curvature vary from the radius of individual collagen fibrils up to almost 1 μm.

We have also noted that the curvature of the platelets is only detectable in sections cut normal to the axes of collagen fibrils; in sections cut parallel to the CF axes, the MPs appear almost perfectly straight or at most gently bowed with very large radii of curvature. From these two facts, we conclude that the overall form of the platelets must be cylindroidal sheets. In earlier studies [15,60] we showed that curved platelets of varying radius of curvature contribute significantly to the strength of bone. In addition, the curvature of these large platelets and the stacks constructed from them allows a larger number of them (per unit volume) to fill the space between collagen fibrils and thus to contribute strength to bone.

Declaration of competing interest

The authors declare there is no conflict of interests.

CRediT authorship contribution statement

H.P. Schwarcz: Writing – review & editing, Writing – original draft, Visualization, Supervision, Methodology, Investigation, Formal analysis, Conceptualization. **Nadine Nassif:** Writing – review & editing, Visualization, Resources, Methodology, Data curation. **Viktoria Kovacs Kis:** Writing – review & editing, Writing – original draft, Visualization, Resources, Investigation, Data curation, Conceptualization.

Acknowledgements

We acknowledge comments on an earlier version of this paper by K. Grandfield. Assistance to VKK was provided by National Research, Development and Innovation Fund Office, Hungary, Grant number K-125100. The authors acknowledge to assistance of Prof. ML Glasser in providing the technical term "developable surface".

References

[1] H.J. Höhling, R. Kreilos, G. Neubauer, A. Boyde, Electron microscopy and electron microscopical measurements of collagen mineralization in hard tissues, Z. Zellforsch. Mikrosk. Anat. 122 (1971) 36–52, doi:10.1007/BF00936115.
[2] W.J. Landis, M.C. Paine, M.J. Glimcher, Electron microscopic observations of bone tissue prepared anhydrously in organic solvents, J. Ultrasruct. Res. 59 (1977) 1–30, doi:10.1016/S0022-5320(77)80025-7.
[3] N. Reznikov, R. Shahar, S. Weiner, Three-dimensional structure of human lamellar bone: the presence of two different materials and new insights into the hierarchical organization, Bone 59 (2014) 93–104, doi:10.1016/j.bone.2013.10.023.
[4] S. Weiner, T. Arad, W. Traub, Crystal organization in rat bone lamellae, FEBS Lett. 285 (1991) 49–54, doi:10.1016/0014-5793(91)80722-F.
[5] M.J. Glimcher, Recent studies of the mineral phase in bone and its possible linkage to the organic matrix by protein-bound phosphate bonds, Philos. Trans. R. Soc. Lond. B. 304 (2017) 479–508.
[6] F. Nudelman, K. Pieterse, A. George, P.H.H. Bomans, H. Friedrich, L.J. Brylka, P.A.J. Hilbers, G. De With, N.A.J.M. Sommerdijk, The role of collagen in bone apatite formation in the presence of hydroxyapatite nucleation inhibitors, Nat. Mater. (2010), doi:10.1038/nmat2875.
[7] S. Weiner, W. Traub, Bone-structure - from angstroms to microns, Faseb J. 6 (1992) 879–885.
[8] A.L. Arsenault, Crystal-collagen relationships in calcified turkey leg tendons visualized by selected-area dark field electron microscopy, Calcif. Tissue Int. (1988), doi:10.1007/BF02555136.
[9] E. Macías-Sánchez, N.V. Tarakina, D. Ivanov, S. Blouin, A.M. Berzlanovich, P. Fratzl, Spherulitic crystal growth drives mineral deposition patterns in collagen-based materials, Adv. Fuct. Mater. (2022) 2200504, doi:10.1002/adfm.202200504.
[10] A. Boyde, Transmission electron microscopy of ion beam thinned dentine, Cell Tissue Res. 152 (1974) 543–550, doi:10.1007/BF00218937.
[11] V. Jantou-Morris, M.A. Horton, D.W. McComb, The nano-morphological relationships between apatite crystals and collagen fibrils in ivory dentine, Biomaterials 31 (2010) 5275–5286, doi:10.1016/j.biomaterials.2010.03.025.
[12] V. Jantou, M. Turmaine, G.D. West, M.A. Horton, D.W. McComb, Focused ion beam milling and ultramicrotomy of mineralised ivory dentine for analytical transmission electron microscopy, Micron 40 (2009) 495–501, doi:10.1016/j.micron.2008.12.002.
[13] E.A. McNally, H.P. Schwarcz, G.A. Botton, A.L. Arsenault, A model for the ultrastructure of bone based on electron microscopy of ion-milled sections, PLoS ONE 7 (2012) 1–12, doi:10.1371/journal.pone.0029258.
[14] R.K. Nalla, A.E. Porter, C. Daraio, A. Minor, V. Radmilovic, E. Stach, A. Tomsia, R. Ritchie, Ultrastructural examination of dentin using focused ion-beam cross-sectioning and transmission electron microscopy, Micron 36 (2005) 672–680.
[15] H.P. Schwarcz, D. Abueidda, I. Jasiuk, The ultrastructure of bone and its relevance to mechanical properties, Front. Phys. (2017) 5, doi:10.3389/fphy.2017.00039.
[16] B.E.J. Lee, L. Luo, K. Grandfield, C.M. Andrei, H.P. Schwarcz, Identification of collagen fibrils in cross sections of bone by electron energy loss spectroscopy (EELS), Micron (2019), doi:10.1016/j.micron.2019.102706.
[17] C. Micheletti, F.A. Shah, A. Palmquist, K. Grandfield, Ultrastructure and nanoporosity of human bone shown with correlative on-axis electron and spectroscopic tomographies, ACS Nano 17 (2023) 24710–24724, doi:10.1021/acsnano.3c04633.
[18] A.K. Nair, A. Gautieri, S.W. Chang, M.J. Buehler, Molecular mechanics of mineralized collagen fibrils in bone, Nat. Commun. 4 (2013) 1–9, doi:10.1038/ncomms2720.
[19] T. Komori, What is the function of osteocalcin? J. Oral Biosci. 62 (2020) 223–227, doi:10.1016/j.job.2020.05.004.

[20] B. Depalle, Z. Qin, S.J. Shefelbine, M.J. Buehler, Large deformation mechanisms, plasticity, and failure of an individual collagen fibril with different mineral content, J. Bone Miner. Res. 31 (2016) 380–390, doi:10.1002/jbmr.2705.
[21] F. Yuan, S.R. Stock, D.R. Haeffner, J.D. Almer, D.C. Dunand, L.C. Brinson, A new model to simulate the elastic properties of mineralized collagen fibril, Biomech. Model. Mechanobiol. 10 (2011) 147–160, doi:10.1007/s10237-010-0223-9.
[22] D. Kim, B. Lee, S. Thomopoulos, Y.S. Jun, The role of confined collagen geometry in decreasing nucleation energy barriers to intrafibrillar mineralization, Nat. Commun. 9 (2018), doi:10.1038/s41467-018-03041-1.
[23] A.C.S. Alcântara, L.C. Felix, D.S. Galvão, P. Sollero, M.S. Skaf, Devising bone molecular models at the nanoscale: from usual mineralized collagen fibrils to the first bone fibers including hydroxyapatite in the extra-fibrillar volume, Materials 15 (2022), doi:10.3390/ma15062274.
[24] H. Alijani, T.J. Vaughan, A multiscale finite element investigation on the role of intra- and extra-fibrillar mineralisation on the elastic properties of bone tissue, J. Mech. Behav. Biomed. Mater. (2022) 129, doi:10.1016/j.jmbbm.2022.105139.
[25] H.P. Schwarcz, D.M. Binkley, L. Luo, K. Grandfield, A search for apatite crystals in the gap zone of collagen fibrils in bone using dark-field illumination, Bone (2020), doi:10.1016/j.bone.2020.115304.
[26] K. Grandfield, V. Vuong, H.P. Schwarcz, Ultrastructure of bone: hierarchical features from nanometer to micrometer scale revealed in focused ion beam sections in the TEM, Calcif. Tissue Int. 103 (2018) 606–616.
[27] S. Pang, H.P. Schwarcz, I. Jasiuk, Interfacial bonding between mineral platelets in bone and its effect on mechanical properties of bone, J. Mech. Behav. Biomed. Mater. (2021) 113, doi:10.1016/j.jmbbm.2020.104132.
[28] A.A. Lloyd, B. Gludovatz, C. Riedel, E.A. Luengo, R. Saiyed, E. Marty, D.G. Lorich, J.M. Lane, R.O. Ritchie, B. Busse, E. Donnelly, Atypical fracture with long-term bisphosphonate therapy is associated with altered cortical composition and reduced fracture resistance, Proc. Natl. Acad. Sci. (2017) 201704460, doi:10.1073/pnas.1704460114.
[29] H.P. Schwarcz, E.A. McNally, G.A. Botton, Dark-field transmission electron microscopy of cortical bone reveals details of extrafibrillar crystals, J. Struct. Biol. (2014) 188, doi:10.1016/j.jsb.2014.10.005.
[30] J.-B. Forien, J. Uzuhashi, T. Ohkubo, K. Hono, L. Luo, H.P. Schwarcz, A.C. Deymier, C. Krywka, C. Fleck, P. Zaslansky, X-ray diffraction and in situ pressurization of dentine apatite reveals nanocrystal modulus stiffening upon carbonate removal, Acta Biomater. (2020), doi:10.1016/j.actbio.2020.09.004.
[31] D.M. Binkley, J. Deering, H. Yuan, A. Gourrier, K. Grandfield, Ellipsoidal mesoscale mineralization pattern in human cortical bone revealed in 3D by plasma focused ion beam serial sectioning, J. Struct. Biol. 212 (2020) 107615, doi:10.1016/j.jsb.2020.107615.
[32] M.D. McKee, D.J. Buss, N. Reznikov, Mineral tessellation in bone and the Stenciling Principle for extracellular matrix mineralization, J. Struct. Biol. 214 (2021) 107823, doi:10.1016/j.jsb.2021.107823.
[33] W.J. Landis, M.J. Song, A. Leith, L. McEwen, B.F. McEwen, Mineral and organic matrix interaction in normally calcifying tendon visualized in three dimensions by high-voltage electron microscopic tomography and graphic image reconstruction, J. Struct. Biol. 110 (1993) 39–54, doi:10.1006/jsbi.1993.1003.
[34] N. Reznikov, M. Bilton, L. Lari, M.M. Stevens, R. Kröger, Fractal-like hierarchical organization of bone begins at the nanoscale, Science (2018) 360, doi:10.1126/science.aao2189.
[35] E. McNally, F. Nan, G.A. Botton, H.P. Schwarcz, Scanning transmission electron microscopic tomography of cortical bone using Z-contrast imaging, Micron (2013) 49, doi:10.1016/j.micron.2013.03.002.
[36] C. Micheletti, A. Hurley, A. Gourrier, A. Palmquist, T. Tang, F.A. Shah, K. Grandfield, Bone mineral organization at the mesoscale: a review of mineral ellipsoids in bone and at bone interfaces, Acta Biomater. 142 (2022) 1–13, doi:10.1016/j.actbio.2022.02.024.
[37] H.R. Wenk, F. Heidelbach, Crystal alignment of carbonated apatite in bone and calcified tendon: results from quantitative texture analysis, Bone 24 (1999) 361–369, doi:10.1016/S8756-3282(98)00192-6.
[38] M.J. Turunen, J.D. Kaspersen, U. Olsson, M. Guizar-Sicairos, M. Bech, F. Schaff, M. Tägil, J.S. Jurvelin, H. Isaksson, Bone mineral crystal size and organization vary across mature rat bone cortex, J. Struct. Biol. (2016), doi:10.1016/j.jsb.2016.07.005.
[39] M. Tzaphlidou, P. Berillis, Collagen fibril diameter in relation to bone site. A quantitative ultrastructural study, Micron 36 (2005) 703–705, doi:10.1016/j.micron.2005.05.012.
[40] J.P. Cassella, P. Barber, A.C. Catterall, S.Y. Ali, A Morphometric analysis of osteoid collagen fibril diameter in osteogenesis imperfecta, Bone (1994), doi:10.1016/8756-3282(94)90296-8.
[41] F. Nudelman, A.J. Lausch, N.A.J.M. Sommerdijk, E.D. Sone, In vitro models of collagen biomineralization, J. Struct. Biol. (2013), doi:10.1016/j.jsb.2013.04.003.
[42] M.J. Olszta, X. Cheng, S.S. Jee, R. Kumar, Y.Y. Kim, M.J. Kaufman, E.P. Douglas, L.B. Gower, Bone structure and formation: a new perspective, Mater. Sci. Eng. R 58 (2007) 77–116, doi:10.1016/j.mser.2007.05.001.
[43] Y. Wang, T. Azaïs, M. Robin, A. Vallée, C. Catania, P. Legriel, G. Pehau-Arnaudet, F. Babonneau, M.M. Giraud-Guille, N. Nassif, The predominant role of collagen in the nucleation, growth, structure and orientation of bone apatite, Nat. Mater. 11 (2012) 724–733, doi:10.1038/nmat3362.
[44] Y. Wang, S. Von Euw, F.M. Fernandes, S. Cassaignon, M. Selmane, G. Laurent, G. Pehau-Arnaudet, C. Coelho, L. Bonhomme-Coury, M.-M. Giraud-Guille, F. Babonneau, T. Azaïs, N. Nassif, Water-mediated structuring of bone apatite, Nat. Mater. 12 (2013) 1144–1153, doi:10.1038/nmat3787.
[45] S. Weiner, P.A. Price, Disaggregation of bone into crystals, Calcif. Tissue Int. 39 (1986) 365–375, doi:10.1007/BF02555173.
[46] J. Moradian-Oldak, S. Weiner, L. Addadi, W.J. Landis, W. Traub, Electron imaging and diffraction study of individual crystals of bone, mineralized tendon and synthetic carbonate apatite, Connect. Tissue Res. 25 (1991) 219–228, doi:10.3109/03008209109029158.
[47] V. Ziv, S. Weiner, Bone crystal sizes: a comparison of transmission electron width broadening techniques, Connect. Tissue Res. 30 (1994) 165–175.
[48] N. Nassif, F. Martineau, O. Syzgantseva, F. Gobeaux, M. Willinger, T. Coradin, S. Cassaignon, T. Azaïs, M.M. Giraud-Guille, In vivo inspired conditions to synthesize biomimetic hydroxyapatite, Chem. Mater. (2010), doi:10.1021/cm903596q.
[49] P. Fratzl, N. Fratzl-Zelman, K. Klaushofer, G. Vogl, K. Koller, Nucleation and growth of mineral crystals in bone studied by small-angle X-ray scattering, Calcif. Tissue Int. 48 (1991) 407–413, doi:10.1007/BF02556454.
[50] Y. Liu, Y.K. Kim, L. Dai, N. Li, S.O. Khan, D.H. Pashley, F.R. Tay, Hierarchical and non-hierarchical mineralisation of collagen, Biomaterials (2011), doi:10.1016/j.biomaterials.2010.10.018.
[51] S. Weiner, W. Traub, Bone structure: from angstroms to microns, FASEB J. 6 (1992) 879–885, doi:10.1096/fasebj.6.3.1740237.
[52] F.A. Shah, K. Ruscsák, A. Palmquist, Transformation of bone mineral morphology: from discrete marquise-shaped motifs to a continuous interwoven mesh, Bone Rep. 13 (2020) 100283, doi:10.1016/j.bonr.2020.100283.
[53] P. Fratzl, H.S. Gupta, O. Paris, A. Valenta, P. Roschger, K. Klaushofer, Diffracting “stacks of cards” - Some thoughts about small-angle scattering from bone, Prog. Colloid Polym. Sci. 130 (2005) 33–39, doi:10.1007/b107343.
[54] A. Gourrier, C. Li, S. Siegel, O. Paris, P. Roschger, K. Klaushofer, P. Fratzl, Scanning small-angle X-ray scattering analysis of the size and organization of the mineral nanoparticles in fluorotic bone using a stack of cards model, J. Appl. Crystallogr. 43 (2010) 1385–1392, doi:10.1107/S0021889810035090.
[55] W. Tong, M.J. Glimcher, J.L. Katz, L. Kuhn, S.J. Eppell, Size and shape of mineralites in young bovine bone measured by atomic force microscopy, in: Calcif. Tissue Int. (2003) 592–598, doi:10.1007/s00223-002-1077-7.
[56] G.E. Fantner, T. Hassenkam, J.H. Kindt, J.C. Weaver, H. Birkedal, L. Pechenik, J.A. Cutroni, G.A.G. Cidade, G.D. Stucky, D.E. Morse, P.K. Hansma, Sacrificial bonds and hidden length dissipate energy as mineralized fibrils separate during bone fracture, Nat. Mater. (2005), doi:10.1038/nmat1428.
[57] D.J. Buss, N. Reznikov, M.D. McKee, Crossfibrillar mineral tessellation in normal and Hyp mouse bone as revealed by 3D FIB-SEM microscopy, J. Struct. Biol. 212 (2020) 107603, doi:10.1016/j.jsb.2020.107603.
[58] J. Silvent, M. Robin, C. Bussola Tovani, Y. Wang, F. Soncin, S. Delgado, T. Azaïs, C. Sassoye, M.M. Giraud-Guille, J.Y. Sire, N. Nassif, Collagen suprafibrillar confinement drives the activity of acidic calcium-binding polymers on apatite mineralization, Biomacromolecules 22 (2021) 2802–2814, doi:10.1021/acs.biomac.1c00206.
[59] N. Reznikov, R. Shahar, S. Weiner, Bone hierarchical structure in three dimensions, Acta Biomater. 10 (2014) 3815–3826, doi:10.1016/j.actbio.2014.05.024.
[60] A. Idkaidek, H. Schwarcz, I. Jasiuk, Modeling of bending and torsional stiffnesses of bone at sub-microscale: effect of curved mineral lamellae, J. Biomech. 123 (2021) 110531, doi:10.1016/j.jbiomech.2021.110531.
[61] Z. Qin, A. Gautieri, A.K. Nair, H. Inbar, M.J. Buehler, Thickness of hydroxyapatite nanocrystal controls mechanical properties of the collagen-hydroxyapatite interface, Langmuir (2012), doi:10.1021/la204052a.